



## Original Paper

## Catalytic oxidation of pentanethiol on basic nitrogen doped carbon hollow spheres derived from waste tires



Jing Luo<sup>a, d</sup>, Wen-Feng Zhang<sup>a</sup>, Yan-Chen Wei<sup>b</sup>, Ji-Xing Liu<sup>a</sup>, Chao Wang<sup>c</sup>, Yi-Ru Zou<sup>b</sup>, Hai-Tao Ju<sup>b</sup>, Li-Ping Mu<sup>b</sup>, Yan-Hong Chao<sup>d</sup>, Hong-Bing Ji<sup>e</sup>, Wen-Shuai Zhu<sup>a, d, \*</sup>

<sup>a</sup> School of Chemistry and Chemical Engineering, Jiangsu University, Zhenjiang, 212013, Jiangsu, China

<sup>b</sup> School of Materials Science and Engineering, Jiangsu University, Zhenjiang, 212013, Jiangsu, China

<sup>c</sup> School of the Environment and Safety Engineering, Jiangsu University, Zhenjiang, 212013, Jiangsu, China

<sup>d</sup> College of Chemical Engineering and Environment, State Key Laboratory of Heavy Oil Processing, China University of Petroleum-Beijing, Changping, 102249, Beijing, China

<sup>e</sup> School of Chemistry, Sun Yat-Sen University, Guangzhou, 510275, Guangdong, China

## ARTICLE INFO

## Article history:

Received 31 May 2021

Accepted 13 August 2021

Available online 12 April 2022

Edited by Xiu-Qiu Peng

## Keywords:

Carbon hollow spheres

Nitrogen-doping

Waste tires

Leavening strategy

Pentanethiol

## ABSTRACT

A series of basic nitrogen doped carbon hollow spheres (p-N-C) catalysts derived from waste tires were prepared by a green, facile and environmental “leavening” strategy for the catalytic oxidation of pentanethiol. Compared to pristine carbon, the p-N-C has a higher surface curvature conducive to the enrichment of substrates, leading to an excellent catalytic performance. This increased surface curvature of p-N-C was fabricated on the synergistic effect of two foaming agents ((NH<sub>4</sub>)<sub>2</sub>C<sub>2</sub>O<sub>4</sub> and NaHCO<sub>3</sub>), and the released gas also endows the spherical shell of p-N-C with a hierarchical porous structure, promoting the accessibility of active sites with pentanethiol. Pyridine-like and pyrrolic-like nitrogen atoms were investigated as reactive sites on the p-N-C to accelerate the electron transfer from sulfur to active surface oxygen and enhance the adsorption/oxidation process. As a result, the optimal p-N-C catalyst exhibits superior adsorption and oxidation performance (99.9%) of pentanethiol, outperforming the “unleavened” catalyst (20.8%). This work offers a new avenue for the fabrication of highly efficient materials for the desulfurization of fuel.

© 2022 The Authors. Publishing services by Elsevier B.V. on behalf of KeAi Communications Co. Ltd. This is an open access article under the CC BY-NC-ND license (<http://creativecommons.org/licenses/by-nc-nd/4.0/>).

## 1. Introduction

Mercaptans, one of the sulfur-containing compounds from fuel, have seriously threatened equipment, ecological environment, and human health (Li et al., 2020; Makarov et al., 2020; Sun et al., 2020a; Yang et al., 2016). Up to date, the merox process has been the universal desulfurization method to remove mercaptans in an industrial application (Sun et al., 2020a). This technique, however, is easy to restrain reactivity because of the accumulation of sulfide in the alkali solution circulation. Consequently, it has already become a significant concern on how to efficiently remove mercaptans from fuel. In this regard, many alternative approaches have been developed to achieve this goal, for instance, photoreaction

(Zheng et al., 2019), oxidation (Makarov et al., 2020; Scott et al., 2019), and adsorption (Meshkat et al., 2018b). Among them, adsorption/oxidation desulfurization has emerged as an intriguing strategy because of its low cost, high efficiency, and facile process. The desulfurization process is that mercaptan is oxidized to disulfide (Eq. n b (1)) (Zhao et al., 2015), and then clean oil is obtained by distillation. The nanoporous carbon-based material, a primary kind of adsorbent used to remove mercaptans from liquids, attracts considerable attention because of its high specific surface area, large pore volume, and adjustable surface properties (Lyu et al., 2020; Meshkat et al., 2018b). Nevertheless, it was found that the pristine carbon-based materials faced several critical issues: (1) insufficient capacities; (2) inadequate active sites and/or the hindrance effect of mass transfer (Tang et al., 2016); (3) massive consumption of ZnCl<sub>2</sub> and KOH (Deng et al., 2015; Li et al., 2018). Therefore, it is highly desirable to develop a new strategy to construct carbon-based materials with abundant active sites for adsorption/oxidation desulfurization of mercaptans.

\* Corresponding author. School of Chemistry and Chemical Engineering, Jiangsu University, Zhenjiang, 212013, Jiangsu, China.

E-mail address: [zhuws@ujs.edu.cn](mailto:zhuws@ujs.edu.cn) (W.-S. Zhu).

Overall reaction of adsorption/oxidation desulfurization:

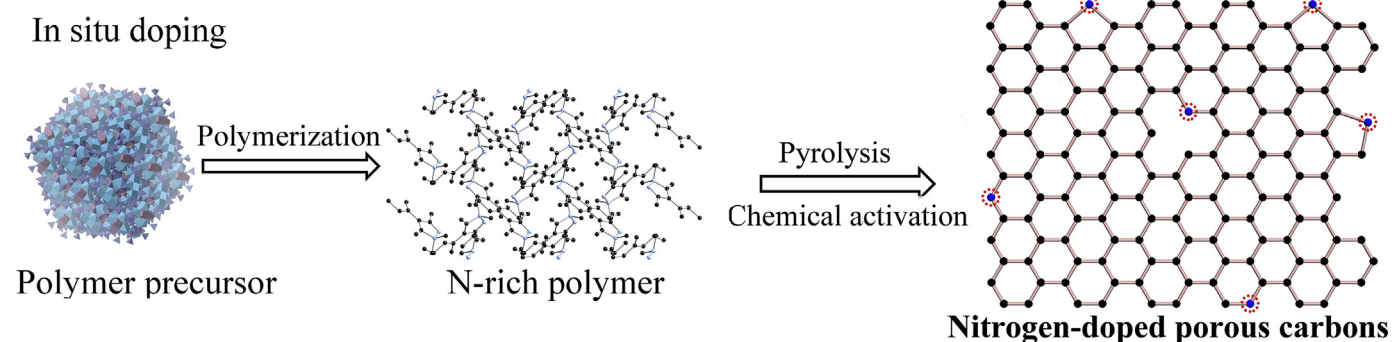


The researchers have devoted much effort to tame the structure and active sites of carbon-based materials, hoping to enhance their desulfurization performances (Huo et al., 2019a, b; Iruretagoyena et al., 2020; Meshkat et al., 2018a; Sun et al., 2020b; Vega et al., 2015). Sun and co-workers prepared nitrogen-doped (N-doped) porous carbons derived from a N-rich polymer precursor and used KOH to improve the porosity of nanoporous carbons. The results indicated that the N doping might act as polar centers to promote the interaction between adsorbent and adsorbate (Tan et al., 2018b). Meshkat et al. employed camphor and urea as raw materials to synthesize a N-doped carbon nanotube (N-CNT) (Meshkat et al., 2018a). Interestingly, the N content directly affects the increased polar or acid-base interaction of carbon material, which exhibited a 45% higher tertiary butyl mercaptan adsorptive capacity than CNT. Besides, Lyu et al. reported that the basic pyridine-like and pyrrolic-like N atoms could be used as reactive sites to accelerate the electron transfer from sulfur to active surface oxygen (Lyu et al., 2020). Nevertheless, it has been realized that these carbon sources used for desulfurization, such as polymer precursor (Tan et al., 2018b), ionic liquid@Al-metal-organic framework (Sarker et al., 2018), polybenzoxazine (Zhao et al., 2018), and biomass (Tan et al., 2018a), show relatively high price or complex synthesis process, which seriously hinder the practical applications of N-doped carbon materials. It is worth noting that the morphology of carbon materials is also crucial in practical applications.

Yao et al. demonstrated that the increased surface curvature is beneficial to enriching substrates (Yao et al., 2019). Carbon hollow spheres in small size have high curvature surfaces providing strong intermolecular interaction to substrates and enhancing the adsorption process. However, the apparent reaction rate of small-sized hollow spheres with high curvature was still hindered by the limited mass transfer. Introducing hierarchical porous structures on the spherical shell is a valuable strategy to avoid the blockage of narrow pores. Meanwhile, interpenetrating channels between the nanospheres can also effectively improve the mass transfer between hollows (Chen et al., 2019). Consequently, fabricating hierarchical porous interpenetrated channels on carbon hollow spheres can further increase the apparent reaction rate and enhance the adsorption/oxidation desulfurization process.

Herein, we present a green and sustainable protocol to realize the upgrading of waste tires into high-effective hierarchical porous N-doped carbon hollow spheres (Fig. 1) using sodium bicarbonate ( $\text{NaHCO}_3$ ) accompanied ammonium oxalate ( $(\text{NH}_4)_2\text{C}_2\text{O}_4$ ) as both nitrogen source and foaming agents. The synergistic effect of two foaming agents directly affects the pore size, specific surface area, and chemical composition of the resultant porous N-doped carbon hollow spheres. Moreover, the adsorption/oxidation performance of the as-constructed materials was investigated via adsorption/oxidation desulfurization for pentanethiol. As expected, the as-prepared N-doped carbon hollow spheres exhibited impressive conversion performance, achieving a sulfur conversion of 99.9% in 3 h at 298 K. This thorough knowledge of N-doped porous carbon hollow spheres upgraded from waste tires can be helpful in the preparation of efficient materials for industrial desulfurization.

## Traditional method



## This work:

### “Leavening” strategy

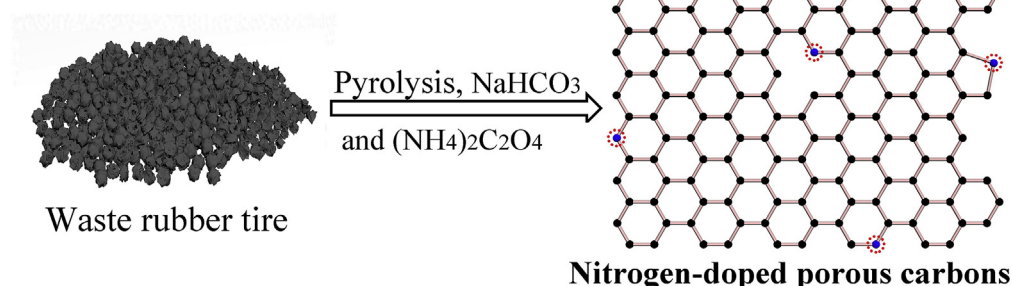


Fig. 1. Schematic representation of the traditional methods and our proposed strategy.

## 2. Experimental section

### 2.1. Materials

Potassium hydroxide (KOH, analytical grade) was purchased from Chengdu Kelong Chemical Reagent Factory. Sodium bicarbonate ( $\text{NaHCO}_3$ , analytical grade), ammonium oxalate ( $(\text{NH}_4)_2\text{C}_2\text{O}_4$ , analytical grade), and activated carbon were used as received from Sinopharm Chemical Reagent Co., Ltd. Pentanethiol (>99.5%) was purchased from TCI (Shanghai) Development Co., Ltd.

### 2.2. Preparation of the carbon hollow spheres

The porous N-doped carbon hollow spheres were synthesized using waste rubber tire particles as the carbon precursors. Waste rubber tire particles and KOH with a mass ratio of 1:2 were firstly dissolved in 50 mL of distilled water and stirred to remove the surface impurities of the waste tire at 60 °C. After that, the mixed solution was filtered, washed, and dried. Then, the resulting black solid,  $\text{NaHCO}_3$ , and  $(\text{NH}_4)_2\text{C}_2\text{O}_4$  were mixed in the mass ratio of 1:0.75:0.1, 1:0.75:0.25, 1:0.75:0.5, and ground well-distributed by the mortar. Finally, the mixture was carbonized in a tubular furnace at 800 °C for 2 h under a  $\text{N}_2$  atmosphere. The prepared porous N-doped carbon hollow spheres were denoted as p-N-C-0.1, p-N-C-0.25, p-N-C-0.5.

Considering the influence of  $\text{NaHCO}_3$  on the structure and composition of carbon material, p-C was also prepared in a similar procedure of p-N-C-0.25 without using  $(\text{NH}_4)_2\text{C}_2\text{O}_4$ . Instead, the mass ratio between the treated waste tire particles and  $\text{NaHCO}_3$  was 1:0.75. The C was obtained by a similar method without adding  $\text{NaHCO}_3$  and  $(\text{NH}_4)_2\text{C}_2\text{O}_4$ .

### 2.3. Characterization of the materials

The morphology of samples was acquired using scanning electron microscopy (SEM, JSM-6010 PLUS/LA) and transmission electron microscopy (TEM, JEOL-JEM-2100).  $\text{N}_2$  adsorption-desorption isotherms were investigated with TriStar II 3020 surface area and porosity analyzer (Micromeritics Instrument Corporation). Elemental composition was collected with an elemental analyzer (FLASH1112A). Fourier-transform infrared (FT-IR) spectra were

investigated with a Nicolet FT-IR spectrophotometer (Nexus 470). Raman spectra were performed with Thermo Scientific DXR. X-ray photoelectron spectrometer (XPS) was operated at VG Miltilab 2000.

### 2.4. Adsorption/oxidation experiments

The model fuels were prepared by mixing pentanethiol with *n*-octane to yield a desired initial sulfur concentration (60 ppm, 72 ppm, 203 ppm, 305 ppm, 500 ppm). The adsorption/oxidation desulfurization experiments were conducted by adding 0.1 g catalyst to a 50 mL glass-stoppered conical flask with 20 mL model fuel and stirring at 150 rpm. The initial and residual sulfur concentrations were analyzed by a gas chromatography-flame photometric detector (GC-FPD).

Dynamic adsorption/oxidation desulfurization tests (fixed bed column, 1.0 g catalyst, 0.1 mL/min, 500 ppm) were performed under 298 K.

The conversion rate of pentanethiol over catalyst was calculated by the following equation:

$$S_{\text{conversion}}(\%) = \frac{(C_0 - C_t)}{C_0} \times 100\% \quad (2)$$

where  $C_0$  and  $C_t$  were the initial sulfur content (ppm) and sulfur content (ppm) at  $t$  min, respectively.

## 3. Results and discussions

### 3.1. Characterization of the carbon hollow spheres

Systematic characterization was investigated to evaluate the effectiveness of the proposed synthesis strategy and clarify the relationship between the adsorption/oxidation desulfurization performance and the structure of these fabricated hierarchical porous N-doped carbon hollow spheres. Initially, the Raman spectra of the C, p-C, and p-N-C-0.25 are presented in Fig. 2. Two peaks centered around 1300 and 1600  $\text{cm}^{-1}$  can be assigned to the D and G bands, respectively (Yang et al., 2005). The D band is assigned to the disorder induced by defect sites on the graphitic plane, and the G band is attributed to the stretching bond of  $\text{sp}^2$  hybridized carbon (Pan et al., 2014; Wang et al., 2015). The ratio of  $I_d/I_g$  can be used to determine the degree of graphitization of the carbon material. With the decrease of  $I_d/I_g$  value, the structural defects of the carbon material decrease, suggesting a high degree of graphitization. As shown in Fig. 2, the order of the  $I_d/I_g$  values of the three carbon materials decreases in the following sequence: C (2.76) > p-C (2.33) > p-N-C-0.25 (2.01), respectively. C atom in the middle of carbon material can be easily incorporated into triple-coordinated N atom because of the suitable match between the triple-coordination characteristic of N atom and  $\text{sp}^2$ -hybridized C atoms (Meshkat et al., 2018a). Therefore, p-N-C-0.25 should possess the highest degree of graphitization.

Considering that this unique etching effect will affect the morphology, the microstructure of the representative p-N-C-0.25 is further studied by TEM (Fig. 3) (Cao et al., 2020b). A striking difference could be noted between p-N-C-0.25 and the bulk carbon counterpart. Compared with C, p-N-C-0.25 additionally exhibits interpenetrated hollow channels (Fig. 3b), which are most likely templated by the gasification of these intermediate products ( $\text{H}_2\text{O}$ ,  $\text{CO}_2$ ,  $\text{NH}_3$ ,  $\text{CO}$ ) generated from the decomposition of  $\text{NaHCO}_3$  and  $(\text{NH}_4)_2\text{C}_2\text{O}_4$  during the calcination process (Deng et al., 2016; Tang et al., 2016). The unique spherical physical structure can provide a sizeable reactive interface in high curvature, which is more conducive to enrich substrates, promoting the accessibility of active sites to pentanethiol, and improving its catalytic oxidation.

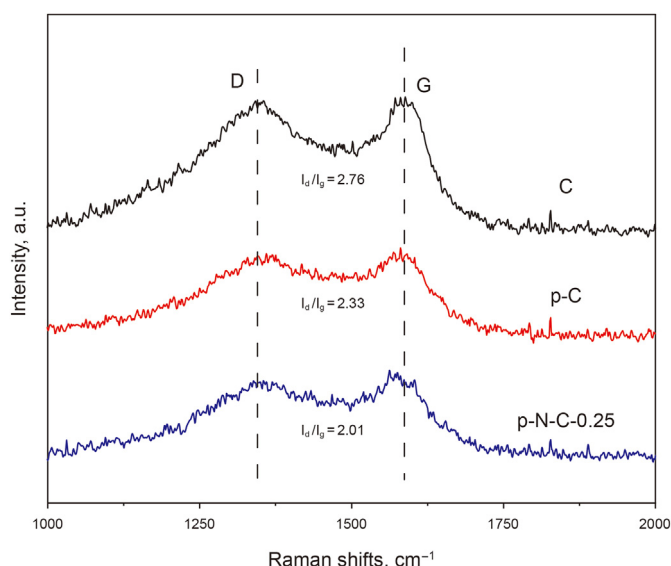


Fig. 2. Raman spectra of C, p-C, and p-N-C-0.25.

The pore structure and pore size distributions of various carbon materials were further investigated by the  $N_2$  adsorption-desorption tests (Fig. 4). According to the IUPAC classification, the curve types of all carbon materials exhibit a hybrid (type II and IV) curve with H3 type hysteresis loop (Chao et al., 2019; Liu et al., 2019a; Nanoti et al., 2009; Zhu et al., 2016). The specific surface areas of C, p-C, and p-N-C-0.25 were 33, 89, and 126  $m^2/g$  (Table 1), respectively. As shown in Fig. 4b, mainly large mesoporous structures over a width of 30 nm could be detected in the C sample. However, on the gasification-templating effect of intermediate products, both the p-C and p-N-C-0.25 had additional microporous and mesoporous structures below a width of 30 nm. Moreover, the mesopores in p-N-C-0.25 had a continuous pore width distribution, corresponding to the interpenetrated hollow channels, as shown in Fig. 3b. This characteristic should be favorable for reducing the diffusion resistance without blocking the pores and accelerating the conversion rates, thereafter enhancing the adsorption/oxidation process for pentanethiol (Dong et al., 2020; Shi et al., 2015). As a result, compared with C, p-N-C-0.25 presents the larger specific

surface area and more porous structure, which could not only promote the nitrogen doping at the edge of p-N-C-0.25, but also provide an abundant reactive interface for the adsorption/oxidation (Liu et al., 2019b; Tan et al., 2018a).

The chemical composition of the as-prepared carbon materials were further investigated. The nitrogen contents of C, p-C, and p-N-C-0.25 were 0.75%, 0.96%, and 1.06%, respectively. The elemental analysis results indicate that the N atoms are successfully introduced into carbon materials by decomposing  $NaHCO_3$  and  $(NH_4)_2C_2O_4$ . As exhibited in the mapping images (Fig. 5), there is a uniform distribution for the C, N, and O elements in the p-N-C-0.25, indicating that the additional nitrogen was successfully dispersed in the porous structure of p-N-C-0.25 (Zhang et al., 2019). To further study the type of doped nitrogen atoms, FT-IR analysis was performed on the as-prepared carbon materials. Several characteristic peaks at 896, 1123, 1384, and 1630  $cm^{-1}$  are observed, which are attributed to the pyrrolic N, graphite N, pyridine oxide, and pyridine N, respectively (Fig. 6a) (Ghasemy et al., 2018; Seredych et al., 2010; Sheng et al., 2011; Wood et al., 2014). These different kinds of N

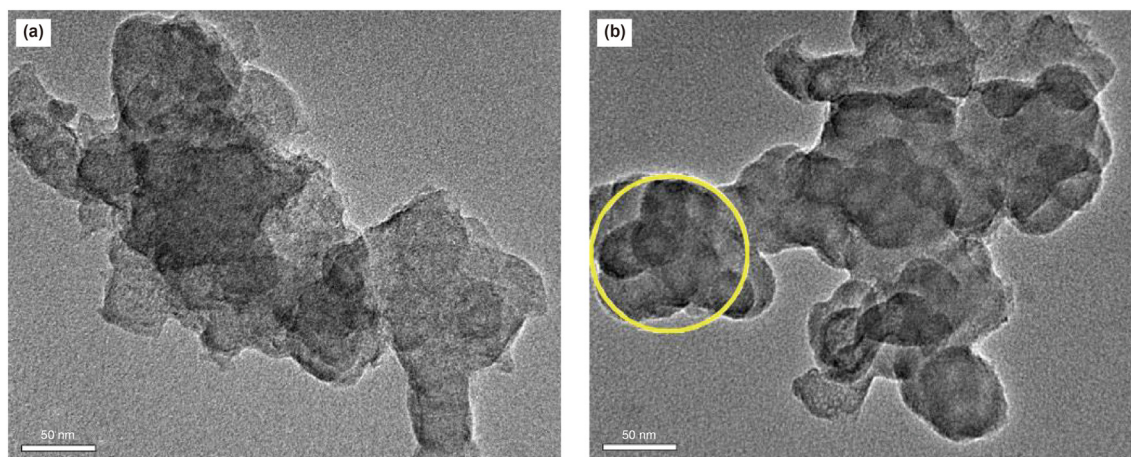


Fig. 3. The TEM images of C (a) and p-N-C-0.25 (b).

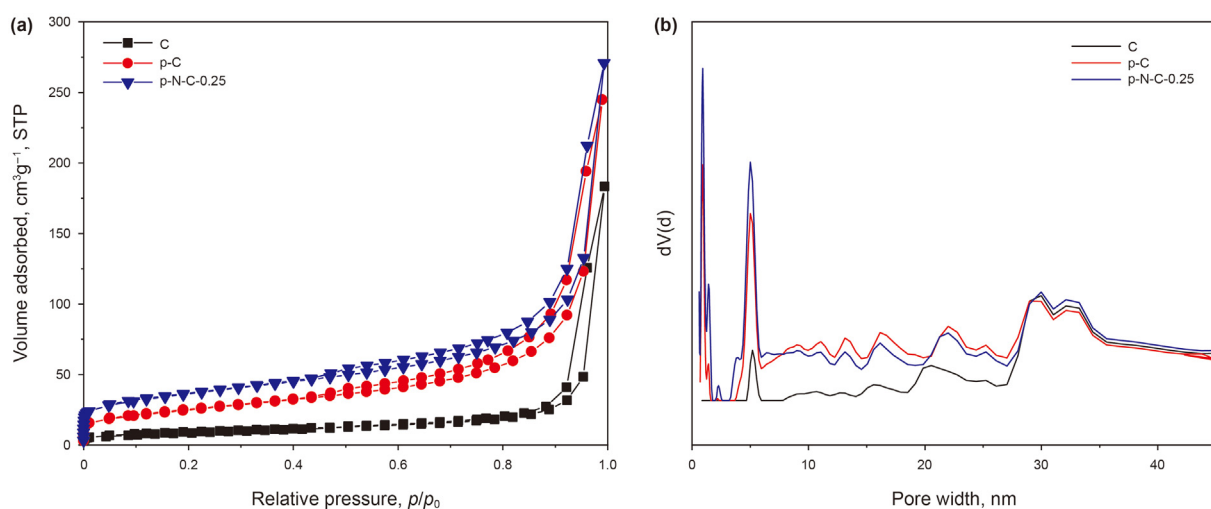


Fig. 4. The  $N_2$  adsorption-desorption isotherms (a) and pore size distributions (b) of C, p-C, and p-N-C-0.25 (the pore size distribution was calculated by quenched solid-state density functional theory (QSDFT) using adsorption curve).

atoms indicate that their positions on carbon materials are different. Except for graphite N, the other kinds of N atoms are located on the vacancy and edge of carbon materials. The specific content of various nitrogen atoms can be further analyzed by XPS characterization to study the influence of etching and pore-forming process on N doping.

XPS is an effective method to detect the surface elemental composition and nitrogen bonding configurations of C, p-C, and p-N-C-0.25 (Cao et al., 2020a). The high-resolution N1s spectra of C and p-N-C-0.25 were deconvoluted into four peaks at around 398.5, 399.8, 401.1, and 402.9 eV for pyridine-like N, pyrrolic-like N, graphite-like N, and oxidized N, respectively (Sheng et al., 2011) (Fig. 6b,d). The surface relative concentration ratios of different forms of nitrogen calculated from the peak fitting of N1s XPS were summarized in Table 2 (Liu et al., 2020). With the introduction of  $(\text{NH}_4)_2\text{C}_2\text{O}_4$ , the area ratio corresponding to pyrrolic-like N in p-N-C-0.25 increases slightly. Therefore,  $\text{NaHCO}_3$  combined with  $(\text{NH}_4)_2\text{C}_2\text{O}_4$  mixed foaming agent could introduce basic pyrrolic-like N into the carbon skeleton of p-N-C-0.25. It is widely accepted that pyridinic-like and pyrrolic-like N of carbon materials have a stronger interaction with sulfur compounds (Meshkat et al., 2018a). Therefore, the adsorption/oxidation performance of p-N-C-0.25 is expected to increase due to the contribution of these doped N atoms and larger specific surface area.

**Table 1**  
The specific surface area and pore size of samples.

| Samples    | Specific Surface area, $\text{m}^2/\text{g}$ | Pore size, nm | Pore volume, $\text{cm}^3/\text{g}$ |
|------------|--|---------------|-------------------------------------|
| C          | 33   | 37.88         | 0.28                                |
| p-C        | 89   | 18.09         | 0.37                                |
| p-N-C-0.25 | 126  | 16.40         | 0.40                                |

### 3.2. Adsorption/oxidation desulfurization performance of carbon materials

In view of the favorable hierarchical porous structure and remarkable modification surface reactivity of the carbon material, the adsorption/oxidation desulfurization performance of N-doped carbon hollow spheres for pentanethiol was evaluated and compared with that of C. As observed in Fig. 7, the N-doped carbon hollow spheres with hierarchical porous structure and larger electronegativity show higher adsorption/oxidation desulfurization performance than that of p-C and C counterparts. Especially, p-N-C-0.25 exhibits the highest adsorption/oxidation conversion rate (99.9%) for pentanethiol, followed by p-N-C-0.1 (98.6%), p-N-C-0.5 (91.7%), p-C (87.5%) and C (20.8%). It is widely recognized that these five factors dominate the adsorption/oxidation process: 1) micropores could offer more active sites (Tan et al., 2018a); 2) the mesopores could reduce the hindrance effect and facilitate mass transfer (Zhang et al., 2020); 3) the hollow-sphere size structure can provide strong intermolecular force between the surface and substrates, which is more conducive to the enrichment of substrates; 4) the N atom and its neighboring C atoms could work as reactive sites for the adsorption acidic pentanethiol and the adsorption mechanism was also ascribed to  $n-\pi$  electron donor-acceptor interactions between S atoms of the pentanethiol and the N-doped atoms (Meshkat et al., 2018a); 5) The basic pyridine-like and pyrrolic-like N atoms can be used as reactive sites to accelerate the electron transfer from sulfur to adsorbent adsorbed active surface oxygen or trace oxygen dissolved in model fuel. Fig. 8 illustrates the adsorption/oxidation mechanism over p-N-C-0.25. The hierarchical porous N doped carbon with synergistic structure and composition, therefore, exhibited excellent adsorption/oxidation desulfurization performance.

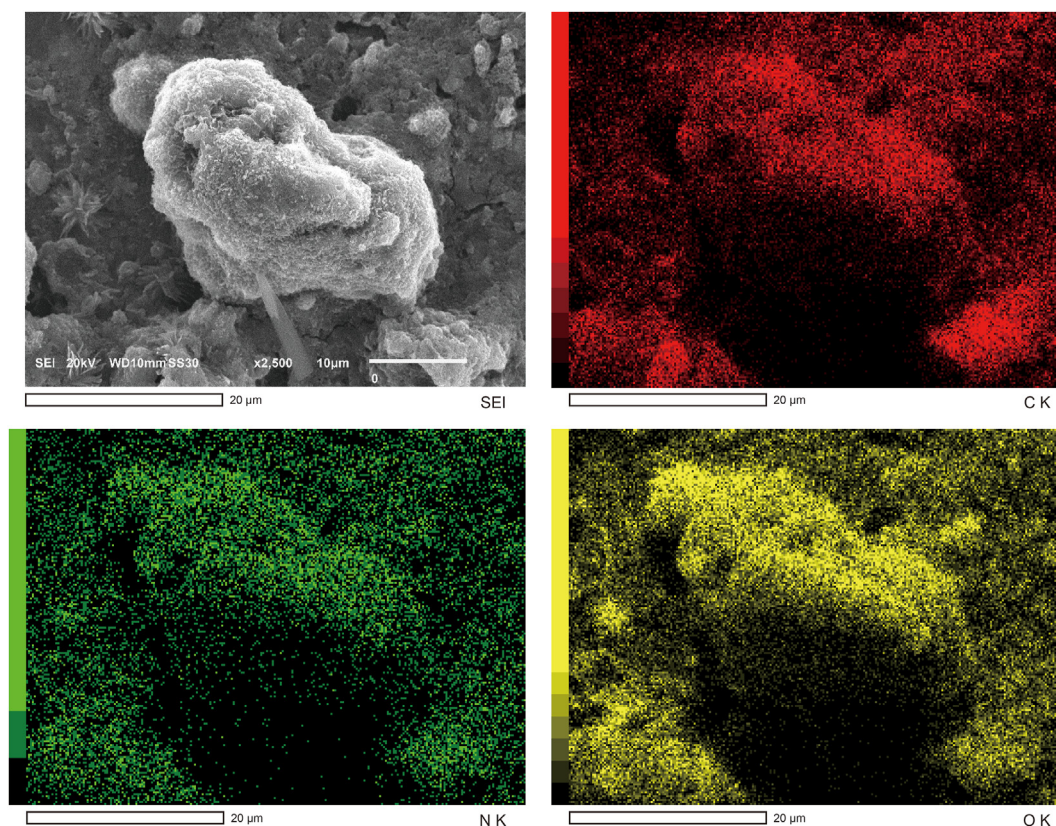


**Fig. 5.** SEM image and mapping of C, N, and O distribution in p-N-C-0.25.

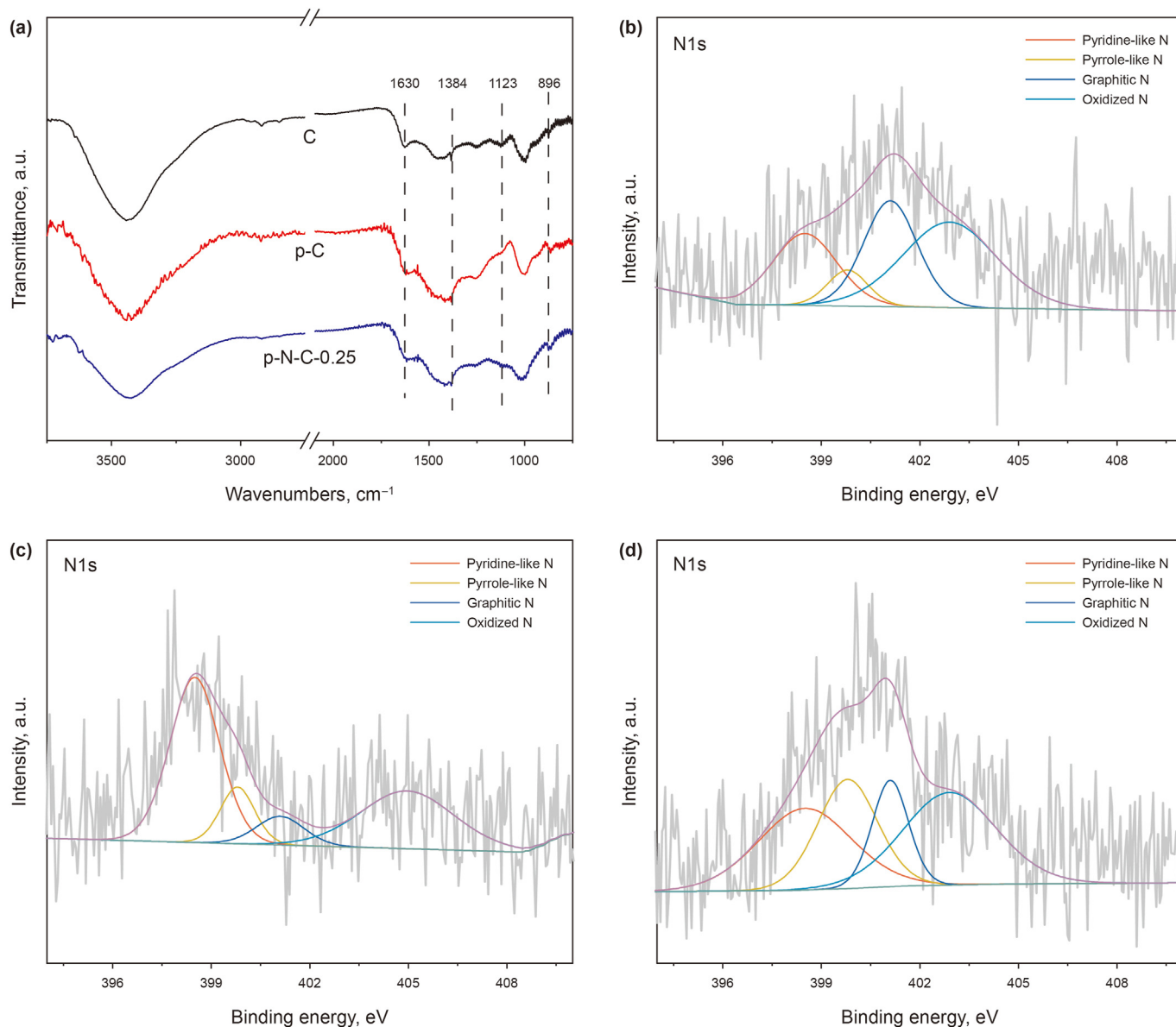


**Fig. 6.** FT-IR spectra of C, p-C, and p-N-C-0.25 (a), high-resolution N1s XPS of C (b), p-C (c), and p-N-C-0.25 (d).

**Table 2**

The area ratio of high-resolution N1s XPS.

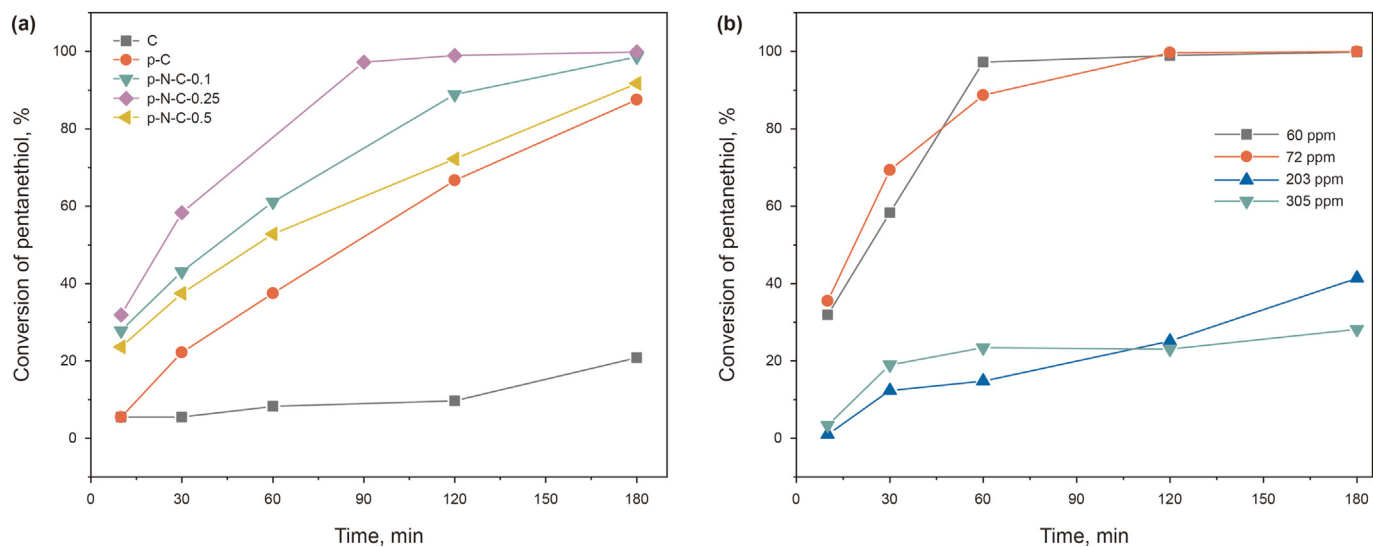
| Samples    | Pyridine-like N, % | Pyrrolic-like N, % | Graphite-like N, % | Oxidized N, % |
|------------|--------------------|--------------------|--------------------|---------------|
| C          | 23                 | 7                  | 29                 | 41            |
| p-C        | 48                 | 12                 | 8                  | 32            |
| p-N-C-0.25 | 29                 | 25                 | 14                 | 32            |

Fig. 7b depicts the influence of initial sulfur concentrations of pentanethiol on the adsorption/oxidation desulfurization of the representative p-N-C-0.25. The conversion rate of pentanethiol was close to 100% when the concentration was below 72 ppm. Further increasing the concentration of pentanethiol, the conversion rate of pentanethiol over p-N-C-0.25 gradually decreases. It indicates that the p-N-C-0.25 can almost completely remove pentanethiol at a concentration of 72 ppm or less. With the increase of the concentration of pentanethiol, the adsorption/oxidation desulfurization performance of p-N-C-0.25 may reach saturation, thereafter the

reduced sulfur content is similar and the adsorption/oxidation conversion rate decreases.

It is well-known that the dynamic adsorption/oxidation desulfurization process plays an essential role in influencing the conversion rate of pentanethiol. Therefore, dynamic adsorption/oxidation desulfurization experiments on different catalysts were performed to explore the adsorption/oxidation performance. As shown in Fig. 9a, after a series of modifications, the adsorption/oxidation performance of carbon materials for pentanethiol increased significantly, especially after introducing basic pyridine-like and pyrrolic-like N atoms, because it can adsorb acidic pentanethiol and catalyze the conversion of pentanethiol. Therefore, the catalytic performance of the p-N-C-0.25 with basic pyridine-like and pyrrolic-like N atoms and larger specific surface area was the best. To further explore the type of sulfide converted, the oxidation products were analyzed by GC-MS, showing that the main product was dipentyl disulfide.

Based on the above observations, it could be concluded that the hierarchical porous N-doped carbon hollow spheres have been



**Fig. 7.** (a) The conversion rate of pentanethiol over carbon materials. Experimental conditions: 72 ppm initial sulfur concentration,  $T = 298\text{ K}$ ,  $V(\text{model fuel}) = 20\text{ mL}$ ,  $m(\text{catalysts}) = 0.1\text{ g}$ , 150 rpm and atmospheric pressure. (b) The adsorption/oxidation conversion rate for different concentrations of pentanethiol. Experimental conditions:  $T = 298\text{ K}$ ,  $V(\text{model fuel}) = 20\text{ mL}$ ,  $m(\text{p-N-C-0.25}) = 0.1\text{ g}$ , 150 rpm and atmospheric pressure.

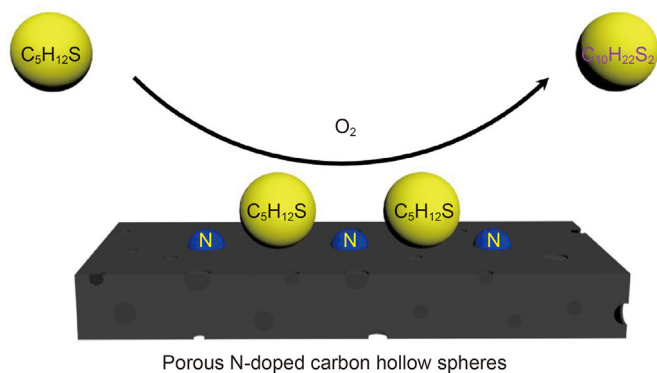


**Fig. 8.** Illustrates the adsorption/oxidation mechanism over p-N-C-0.25.

successfully prepared by the foaming agents assisted “leavening” strategy, which endows these materials with hierarchical porous structure and abundant active sites. This strategy not only reduces the diffusion resistance of reactant molecules, but also facilitates the mass transfer. For the two foaming agents,  $\text{NaHCO}_3$  was mainly used for pore-forming and carbon atom etching, which was conducive to the insertion of N atom in  $(\text{NH}_4)_2\text{C}_2\text{O}_4$  into the carbon skeleton. More importantly, the small size hollow-sphere structure with high surface curvature can be conducive to the enrichment of substrates. N atoms and their neighboring C atoms serving as the reactive sites positively enhance interaction with sulfur compounds. Both factors mentioned above collectively contributed to the excellent desulfurization performances of hierarchical porous N-doped carbon materials.

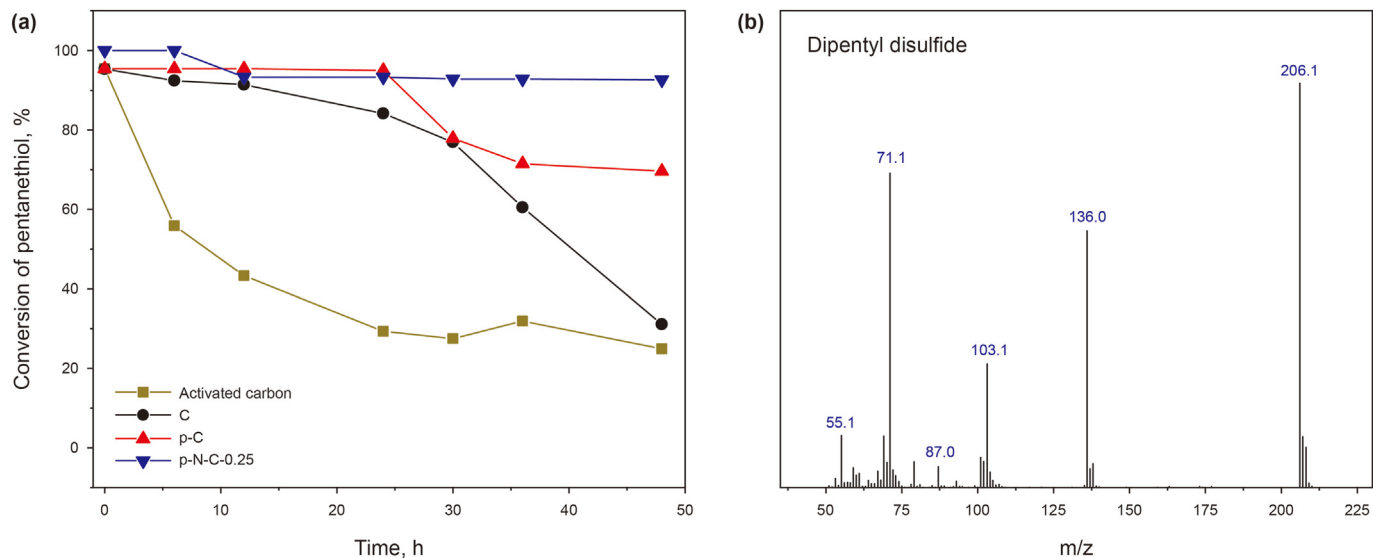


**Fig. 9.** (a) Dynamic adsorption/oxidation desulfurization experiments on different kinds of catalysts. Experimental conditions: 500 ppm initial sulfur concentration, flow rate (model fuel) = 0.1 mL/min,  $m(\text{catalyst}) = 1.0\text{ g}$ , 298 K and atmospheric pressure. (b) GC-MS analysis of the sulfides in the reaction process.

## 4. Conclusions

In summary, through the designed “leavening” strategy, a new approach to upgrade the waste tires to high-value catalysts was made in the synergistic effect of two foaming agents. The results of elemental analysis, FT-IR, and XPS show that N atoms are successfully incorporated onto the p-N-C materials. The N<sub>2</sub> adsorption and desorption results reveal that the specific surface area of the p-N-C-0.25 with hierarchical porous structures is four times that of the untreated carbon material. Because of this, the pyridine-like and pyrrolic-like N atoms could work as reactive sites to accelerate the electron transfer from sulfur to active surface oxygen for the adsorption/oxidation of acidic pentanethiol. Among different catalysts, the conversion rate of pentanethiol over p-N-C-0.25 was 99.9%. These hierarchical porous N-doped carbon hollow spheres synthesized by the “leavening” strategy provide new opportunities for desulfurization and lay a foundation for the innovation and design of other high-value products from solid wastes.

## Declaration of competing interest

The authors declare that they have no known competing financial interests or personal relationships that could have appeared to influence the work reported in this paper.

## Acknowledgments

This work was financially supported by the National Natural Science Foundation of China (Nos. 21722604, 21878133, and 22002050), China Postdoctoral Science Foundation (No. 2020M671365), Postgraduate Research & Practice Innovation Program of Jiangsu Province (No. KYCX20\_3039).

## References

- Cao, Y., Fu, W., Ren, Z., et al., 2020a. Tailoring electronic properties and kinetics behaviors of Pd/N-CNTs catalysts for selective hydrogenation of acetylene. *AlChE J.* 66, e16857. <https://doi.org/10.1002/aic.16857>.
- Cao, Y., Zhang, H., Ji, S., et al., 2020b. Adsorption site regulation to guide atomic design of Ni-Ga catalysts for acetylene semi-hydrogenation. *Angew. Chem. Int. Ed.* 59, 11647–11652. <https://doi.org/10.1002/anie.202004966>.
- Chao, Y., Ju, H., Luo, J., et al., 2019. Synthesis of porous carbon via a waste tire leavening strategy for adsorptive desulfurization. *RSC Adv.* 9, 30575–30580. <https://doi.org/10.1039/c9ra06195a>.
- Chen, Z., Hu, Z., Wang, J., et al., 2019. Synthesis of mesoporous silica-carbon microspheres via self-assembly and in-situ carbonization for efficient adsorption of Di-n-butyl phthalate. *Chem. Eng. J.* 369, 854–862. <https://doi.org/10.1016/j.cej.2019.03.128>.
- Deng, J., Li, M., Wang, Y., 2016. Biomass-derived carbon: synthesis and applications in energy storage and conversion. *Green Chem.* 18, 4824–4854. <https://doi.org/10.1039/c6gc01172a>.
- Deng, J., Xiong, T., Xu, F., et al., 2015. Inspired by bread leavening: one-pot synthesis of hierarchically porous carbon for supercapacitors. *Green Chem.* 17, 4053–4060. <https://doi.org/10.1039/c5gc00523j>.
- Dong, L., Miao, G., Ren, X., et al., 2020. Desulfurization kinetics and regeneration of silica gel-supported TiO<sub>2</sub> extrudates for reactive adsorptive desulfurization of real diesel. *Ind. Eng. Chem. Res.* 59, 10130–10141. <https://doi.org/10.1021/acs.iecr.0c00942>.
- Ghasemy, E., Motejjaded, H.B., Rashidi, A., et al., 2018. N-doped CNT nanocatalyst prepared from camphor and urea for gas phase desulfurization: experimental and DFT study. *J. Taiwan Inst. Chem. Eng.* 85, 121–131. <https://doi.org/10.1016/j.jtice.2017.12.026>.
- Huo, Q., Li, J., Liu, G., et al., 2019a. Adsorption desulfurization performances of Zn/Co porous carbons derived from bimetal-organic frameworks. *Chem. Eng. J.* 362, 287–297. <https://doi.org/10.1016/j.cej.2019.01.050>.
- Huo, Q., Li, J., Qi, X., et al., 2019b. Cu, Zn-embedded MOF-derived bimetallic porous carbon for adsorption desulfurization. *Chem. Eng. J.* 378, 122106. <https://doi.org/10.1016/j.cej.2019.122106>.
- Iruretagoyena, D., Bikane, K., Sunny, N., et al., 2020. Enhanced selective adsorption desulfurization on CO<sub>2</sub> and steam treated activated carbons: equilibria and kinetics. *Chem. Eng. J.* 379, 122356. <https://doi.org/10.1016/j.cej.2019.122356>.
- Li, X., Zhu, H., Liu, C., et al., 2018. Synthesis, modification, and application of hollow mesoporous carbon microspheres for adsorptive desulfurization. *Ind. Eng. Chem. Res.* 57, 15020–15030. <https://doi.org/10.1021/acs.iecr.8b02780>.

- Li, Y.X., Shen, J.X., Peng, S.S., et al., 2020. Enhancing oxidation resistance of Cu(I) by tailoring microenvironment in zeolites for efficient adsorptive desulfurization. *Nat. Commun.* 11, 3206. <https://doi.org/10.1038/s41467-020-17042-6>.
- Liu, F., Yi, X., Chen, W., et al., 2019a. Developing two-dimensional solid superacids with enhanced mass transport, extremely high acid strength and superior catalytic performance. *Chem. Sci.* 10, 5875–5883. <https://doi.org/10.1039/c9sc01988j>.
- Liu, J., Wang, L., Okejiri, F., et al., 2020. Deep understanding of strong metal interface confinement: a journey of Pd/FeOx catalysts. *ACS Catal.* 10, 8950–8959. <https://doi.org/10.1021/acscatal.0c01447>.
- Liu, J., Zhao, Z., Xu, C., et al., 2019b. Structure, synthesis, and catalytic properties of nanosize cerium-zirconium-based solid solutions in environmental catalysis. *Chin. J. Catal.* 40, 1438–1487. [https://doi.org/10.1016/s1872-2067\(19\)63400-5](https://doi.org/10.1016/s1872-2067(19)63400-5).
- Lyu, Y., Liu, X., Liu, W., et al., 2020. Adsorption/oxidation of ethyl mercaptan on Fe-N-modified active carbon catalyst. *Chem. Eng. J.* 393, 124680. <https://doi.org/10.1016/j.cej.2020.124680>.
- Makarov, S.G., Ketkov, S.Y., Wöhrle, D., 2020. A planar binuclear cobalt(ii) phthalocyanine as a highly efficient catalyst for the oxidation of a mercaptan. *Chem. Commun.* 56, 5653–5656. <https://doi.org/10.1039/d0cc01653e>.
- Meshkat, S.S., Rashidi, A., Tavakoli, O., 2018a. Removal of mercaptan from natural gas condensate using N-doped carbon nanotube adsorbents: kinetic and DFT study. *J. Nat. Gas Sci. Eng.* 55, 288–297. <https://doi.org/10.1016/j.jngse.2018.04.036>.
- Meshkat, S.S., Tavakoli, O., Rashidi, A., et al., 2018b. Adsorptive mercaptan removal of liquid phase using nanoporous graphene: equilibrium, kinetic study and DFT calculations. *Ecotoxicol. Environ. Saf.* 165, 533–539. <https://doi.org/10.1016/j.ecoenv.2018.08.110>.
- Nanoti, A., Dasgupta, S., Goswami, A.N., et al., 2009. Mesoporous silica as selective sorbents for removal of sulfones from oxidized diesel fuel. *Microporous Mesoporous Mater.* 124, 94–99. <https://doi.org/10.1016/j.micromeso.2009.04.040>.
- Pan, F., Cao, Z., Zhao, Q., et al., 2014. Nitrogen-doped porous carbon nanosheets made from biomass as highly active electrocatalyst for oxygen reduction reaction. *J. Power Sources* 272, 8–15. <https://doi.org/10.1016/j.jpowsour.2014.07.180>.
- Sarker, M., An, H.J., Yoo, D.K., et al., 2018. Nitrogen-doped porous carbon from ionic liquid@Al-metal-organic framework: a prominent adsorbent for purification of both aqueous and non-aqueous solutions. *Chem. Eng. J.* 338, 107–116. <https://doi.org/10.1016/j.cej.2017.12.157>.
- Scott, D.W., Myers, D.L., Hill, H., et al., 2019. Sodium cobalt(II) tetrasulfophthalocyanine and catalytic oxidation of ethanethiol. *Fuel* 242, 573–579. <https://doi.org/10.1016/j.fuel.2019.01.055>.
- Seredych, M., Hulicova-Jurcakova, D., Bandosz, T.J., 2010. Effect of the incorporation of nitrogen to a carbon matrix on the selectivity and capacity for adsorption of dibenzothiophenes from model diesel fuel. *Langmuir* 26, 227–233. <https://doi.org/10.1021/la902059y>.
- Sheng, Z.H., Shao, L., Chen, J.J., et al., 2011. Catalyst-free synthesis of nitrogen-doped graphene via thermal annealing graphite oxide with melamine and its excellent electrocatalysis. *ACS Nano* 5, 4350–4358. <https://doi.org/10.1021/nn103584t>.
- Shi, Y., Zhang, X., Liu, G., 2015. Activated carbons derived from hydrothermally carbonized sucrose: remarkable adsorbents for adsorptive desulfurization. *ACS Sustainable Chem. Eng.* 3, 2237–2246. <https://doi.org/10.1021/acssuschemeng.5b00670>.
- Sun, D., Zhao, Y., Cao, Y., et al., 2020a. Investigation on the interaction mechanism of the solvent extraction for mercaptan removal from liquefied petroleum gas. *Energy Fuels* 34, 4788–4798. <https://doi.org/10.1021/acs.energyfuels.0c00537>.
- Sun, X.L., Liu, Z., Cheng, Z.L., 2020b. Design and fabrication of in-situ N-doped paper-like carbon nanofiber film for thiophene removal from a liquid model fuel. *J. Hazard. Mater.* 389, 121879. <https://doi.org/10.1016/j.jhazmat.2019.121879>.
- Tan, P., Jiang, Y., Sun, L.B., et al., 2018a. Design and fabrication of nanoporous adsorbents for the removal of aromatic sulfur compounds. *J. Mater. Chem. A* 6, 23978–24012. <https://doi.org/10.1039/c8ta09184f>.
- Tan, P., Xue, D.M., Zhu, J., et al., 2018b. Hierarchical N-doped carbons from designed N-rich polymer: adsorbents with a record-high capacity for desulfurization. *AlChE J.* 64, 3786–3793. <https://doi.org/10.1002/aic.16357>.
- Tang, M., Deng, J., Li, M., et al., 2016. 3D-interconnected hierarchical porous N-doped carbon supported ruthenium nanoparticles as an efficient catalyst for toluene and quinoline hydrogenation. *Green Chem.* 18, 6082–6090. <https://doi.org/10.1039/c6gc01858k>.
- Vega, E., Sanchez-Polo, M., Gonzalez-Olmos, R., et al., 2015. Adsorption of odorous sulfur compounds onto activated carbons modified by gamma irradiation. *J. Colloid Interface Sci.* 457, 78–85. <https://doi.org/10.1016/j.jcis.2015.06.037>.
- Wang, M., Lai, Y., Fang, L., et al., 2015. N-doped porous carbon derived from biomass as an advanced electrocatalyst for aqueous aluminium/air battery. *Int. J. Hydrogen Energy* 40, 16230–16237. <https://doi.org/10.1016/j.ijhydene.2015.09.054>.
- Wood, K.N., O’Hayre, R., Pylypenko, S., 2014. Recent progress on nitrogen/carbon structures designed for use in energy and sustainability applications. *Energy Environ. Sci.* 7, 1212–1249. <https://doi.org/10.1039/c3ee44078h>.
- Yang, C.M., Noguchi, H., Murata, K., et al., 2005. Highly ultramicroporous single-walled carbon nanohorn assemblies. *Adv. Mater.* 17, 866–870. <https://doi.org/10.1002/adma.200400712>.
- Yang, S., Li, Y., Wang, L., et al., 2016. Use of peroxy monosulfate in wet scrubbing process for efficient odor control. *Sep. Purif. Technol.* 158, 80–86. <https://doi.org/10.1016/j.seppur.2015.12.010>.

- Yao, D., Wang, Y., Hassan-Legault, K., et al., 2019. Balancing effect between adsorption and diffusion on catalytic performance inside hollow nano-structured catalyst. *ACS Catal.* 9, 2969–2976. <https://doi.org/10.1021/acscatal.9b00282>.
- Zhang, X.M., Zhang, Z.H., Zhang, B.H., et al., 2019. Synergistic effect of Zr-MOF on phosphomolybdic acid promotes efficient oxidative desulfurization. *Appl. Catal. B: Environ.* 256, 117804. <https://doi.org/10.1016/j.apcatb.2019.117804>.
- Zhang, Y., Ji, G., Li, C., et al., 2020. Templating synthesis of hierarchical porous carbon from heavy residue of tire pyrolysis oil for methylene blue removal. *Chem. Eng. J.* 390, 124398. <https://doi.org/10.1016/j.cej.2020.124398>.
- Zhao, R., Jin, Z., Wang, J., et al., 2018. Adsorptive desulfurization of model fuel by S, N-codoped porous carbons based on polybenzoxazine. *Fuel* 218, 258–265. <https://doi.org/10.1016/j.fuel.2018.01.043>.
- Zhao, S., Yi, H., Tang, X., et al., 2015. Methyl mercaptan removal from gas streams using metal-modified activated carbon. *J. Clean. Prod.* 87, 856–861. <https://doi.org/10.1016/j.jclepro.2014.10.001>.
- Zheng, T., Liu, B., Wang, A., et al., 2019. Degradation of methyl mercaptan by a microwave-induced photoreaction process. *Chem. Eng. J.* 368, 369–376. <https://doi.org/10.1016/j.cej.2019.02.156>.
- Zhu, W., Gao, X., Li, Q., et al., 2016. Controlled gas exfoliation of boron nitride into few-layered nanosheets. *Angew. Chem. Int. Ed.* 55, 10766–10770. <https://doi.org/10.1002/anie.201605515>.